

Dissecting ion-specific dielectric spectra of sodium-halide solutions into solvation water and ionic contributions

Klaus F. Rinne, Stephan Gekle, and Roland R. Netz

Citation: *The Journal of Chemical Physics* **141**, 214502 (2014); doi: 10.1063/1.4901927

View online: <http://dx.doi.org/10.1063/1.4901927>

View Table of Contents: <http://scitation.aip.org/content/aip/journal/jcp/141/21?ver=pdfcov>

Published by the [AIP Publishing](#)

Articles you may be interested in

Dielectric spectra broadening as a signature for dipole-matrix interaction. IV. Water in amino acids solutions
J. Chem. Phys. **140**, 135104 (2014); 10.1063/1.4869542

Stokes shift dynamics of ionic liquids: Solute probe dependence, and effects of self-motion, dielectric relaxation frequency window, and collective intermolecular solvent modes
J. Chem. Phys. **139**, 164503 (2013); 10.1063/1.4825195

Electrolytes in a nanometer slab-confinement: Ion-specific structure and solvation forces
J. Chem. Phys. **133**, 164511 (2010); 10.1063/1.3490666

Dielectric relaxation of electrolyte solutions using terahertz transmission spectroscopy
J. Chem. Phys. **116**, 8469 (2002); 10.1063/1.1468888

Dielectric response of concentrated NaCl aqueous solutions: Molecular dynamics simulations
J. Chem. Phys. **115**, 1448 (2001); 10.1063/1.1381055



Dissecting ion-specific dielectric spectra of sodium-halide solutions into solvation water and ionic contributions

Klaus F. Rinne,¹ Stephan Gekle,² and Roland R. Netz¹

¹*Fachbereich Physik, Freie Universität Berlin, 14195 Berlin, Germany*

²*Physikalisches Institut, Universität Bayreuth, 95440 Bayreuth, Germany*

(Received 1 July 2014; accepted 23 October 2014; published online 1 December 2014)

Using extensive equilibrium molecular dynamics simulations we determine the dielectric spectra of aqueous solutions of NaF, NaCl, NaBr, and NaI. The ion-specific and concentration-dependent shifts of the static dielectric constants and the dielectric relaxation times match experimental results very well, which serves as a validation of the classical and non-polarizable ionic force fields used. The purely ionic contribution to the dielectric response is negligible, but determines the conductivity of the salt solutions. The ion-water cross correlation contribution is negative and reduces the total dielectric response by about 5%-10% for 1 M solutions. The dominating water dielectric response is decomposed into different water solvation shells and ion-pair configurations, by this the spectral blue shift and the dielectric decrement of salt solutions with increasing salt concentration is demonstrated to be primarily caused by first-solvation shell water. With rising salt concentration the simulated spectra show more pronounced deviations from a single-Debye form and can be well described by a Cole-Cole fit, in quantitative agreement with experiments. Our spectral decomposition into ionic and different water solvation shell contributions does not render the individual contributions more Debye-like, this suggests the non-Debye-like character of the dielectric spectra of salt solutions not to be due to the superposition of different elementary relaxation processes with different relaxation times. Rather, the non-Debye-like character is likely to be an inherent spectral signature of solvation water around ions. © 2014 AIP Publishing LLC. [<http://dx.doi.org/10.1063/1.4901927>]

I. INTRODUCTION

Water interacts with solutes differently than with other water molecules, which influences the electromagnetic response properties of aqueous solutions and therefore leads to distinct signatures of solvation water and bulk water in absorption spectra. This makes spectroscopy a preferred method for the study of the mechanism of how water solvates polar as well as nonpolar solutes. Dielectric relaxation spectroscopy is a powerful experimental tool to measure the dielectric susceptibility of aqueous solutions in the GHz range and allows to resolve very slow solvation processes.¹ This frequency range is accessible to equilibrium molecular dynamics (MD) simulations which therefore allows in principle for a detailed comparison of simulated and experimental spectra. Robust experimental dielectric spectra are available for solutions of the salts NaF, NaCl, NaBr, and NaI from the Buchner group,²⁻⁴ which by comparison allow to infer ion-specific effects on the static as well as dynamic dielectric properties in an insightful manner. A number of simulation studies calculated dielectric spectra of salt solutions and in particular analyzed the various water, ions, and ion-water cross contributions to the total spectrum.⁵⁻¹³ Surprisingly, no explicit comparison between simulated and experimental dielectric spectra was undertaken, and also the influence of ion-specific effects on dielectric spectra was not addressed in previous simulation work. Only for aqueous saccharide solutions concentration dependent spectra from experiments and simulation were quantitatively compared.¹⁴

This is curious since the decomposition of experimentally measured dielectric spectra into individual contributions stemming from water and ions is challenging and can only be accomplished by fitting the spectra to heuristic sum formulas, assuming that one knows the functional form of the individual spectral contributions and that simple superposition is valid.

In contrast, the full polarization auto-correlation function, which is related to the dielectric spectrum via Fourier transformation, can be straightforwardly decomposed into different molecular contributions in MD simulations. Consequently, if the statistics are robust and the force fields are validated, MD simulations can help to answer central questions related to the range over which ions are able to perturb the water structure and dynamics.¹⁵⁻¹⁷ Other pertinent open questions are whether ion-water polarization cross-correlations enhance or suppress dielectric absorption and to what degree ion-polarization auto-correlations contribute to the static dielectric constant.

We in this paper report on extensive MD simulations for NaF, NaCl, NaBr, and NaI salt solutions. The dielectric spectra show a significant blue shift and a simultaneous decrease of the static dielectric constant with increasing salt concentration and increasing anion size, in almost quantitative agreement with experimental data.²⁻⁴ This serves as a validation of the non-polarizable force fields employed and of the technique we use in order to extract the spectral information from the simulation trajectories. The purely ionic contribution to the dielectric response is negligible, the ion-water cross correlation contribution however is negative and reduces the total

dielectric response by about 5%-10% for 1 M solutions. By a separate analysis of the dielectric contribution from consecutive water solvation shells around ions we demonstrate that the salt-induced effects on the dielectric spectra and in particular the salient blue shift primarily stem from the first solvation shell around ions. This is in agreement with the recent interpretation of THz experiments that probe the collective water motion around ions in a different frequency regime.¹⁸

With rising salt concentration the simulated spectra show more pronounced deviations from a single-Debye form, as quantified by the exponent α of a Cole-Cole fit, this is in quantitative agreement with experimental spectra. Our spectral decomposition into ionic and different water solvation shell contributions does not render the individual contributions more Debye-like, this suggests that the non-Debye-like character of the total dielectric spectra of salt solutions is not due to the superposition of different elementary Debye-like relaxation processes with different relaxation times. Rather, we conclude that the non-Debye-like character of salt solution spectra is an inherent signature of the first water solvation shell around ions.

Our paper is structured in the following way: In Sec. II, we discuss our simulation methods. We validate our methods by comparison of the total dielectric spectra with experimental data in Sec. III, and in Sec. IV we discuss the spectral decomposition results.

II. METHODS

A. Dielectric response functions

The complex frequency-dependent dielectric susceptibility $\chi(f) = \chi'(f) - i\chi''(f)$ relates the total system polarization $\vec{P}(f)$ to the electric field $\vec{E}(f)$ via the linear-response relation $\vec{P}(f) = \chi(f)\epsilon_0\vec{E}(f)$, where ϵ_0 is the vacuum permittivity. According to the fluctuation dissipation theorem $\chi(f)$ follows from the autocorrelation of equilibrium polarization fluctuations via^{19,20}

$$\chi(f) = -\frac{1}{3Vk_B T \epsilon_0} \int_0^\infty e^{-2\pi i f t} \langle \vec{P}(0) \dot{\vec{P}}(t) \rangle dt, \quad (1)$$

where $\dot{\vec{P}}(t)$ denotes the time derivative of the time-dependent total polarization $\vec{P}(t)$, V is the system volume, and $k_B T$ is the thermal energy. Equation (1) thus allows to obtain the complete susceptibility spectrum from one simulation trajectory in equilibrium. Note that for a salt solution the total polarization consists of the water polarization \vec{P}_W and the ionic polarization \vec{P}_I according to $\vec{P} = \vec{P}_W + \vec{P}_I$. In a periodic simulation box, it is convenient to express the ionic polarization in terms of the ionic current \vec{J}_I via $\vec{J}_I(t) = d\vec{P}_I(t)/dt$. The susceptibility has a low-frequency diverging imaginary part due to the ionic DC-conductivity, what is typically experimentally reported is the DC-conductivity corrected dielectric signal $\Delta\chi(f) = \chi(f) + i\sigma_0/(2\pi f)$ that displays regular behavior in the low-frequency limit, where $\sigma_0 = \sigma(f=0)$ is the static ionic conductivity.

The frequency-dependent ionic conductivity $\sigma(f) = \sigma'(f) - i\sigma''(f)$ by definition relates the electric current due

to free ionic charges with the applied electric field according to $\vec{J}_I(f) = \sigma(f)\epsilon_0\vec{E}(f)$ and can be calculated from the polarization-current cross correlations via²¹

$$\sigma(f) = \frac{1}{3Vk_B T \epsilon_0} \int_0^\infty e^{-2\pi i f t} \langle \vec{J}_I(0) \dot{\vec{P}}(t) \rangle dt. \quad (2)$$

By defining the auto and cross-correlation functions of the water polarization and ionic current as

$$\phi_W(t) = \frac{\langle \vec{P}_W(0) \cdot \vec{P}_W(t) \rangle}{3Vk_B T \epsilon_0}, \quad (3)$$

$$\phi_{IW}(t) = \frac{1}{2} \frac{\langle \vec{P}_W(0) \cdot \vec{J}_I(t) - \vec{J}_I(0) \cdot \vec{P}_W(t) \rangle}{3Vk_B T \epsilon_0}, \quad (4)$$

$$\phi_I(t) = \frac{\langle \vec{J}_I(0) \cdot \vec{J}_I(t) \rangle}{3Vk_B T \epsilon_0}, \quad (5)$$

we can express the frequency-dependent ionic conductivity as a sum of a pure ionic term σ_I and an ion-water cross correlation term σ_{IW} ,

$$\sigma(f) = \sigma_{IW}(f) + \sigma_I(f), \quad (6)$$

$$\sigma_{IW}(f) = -i2\pi f \int_0^\infty e^{-2\pi i f t} \phi_{IW}(t) dt, \quad (7)$$

$$\sigma_I(f) = \int_0^\infty e^{-2\pi i f t} \phi_I(t) dt. \quad (8)$$

It follows that the static conductivity is determined by the pure ionic term and can be written as $\sigma(f=0) = \sigma_I(f=0) = \int_0^\infty \phi_I(t) dt$. The regularized susceptibility $\Delta\chi(f)$ can be decomposed into three separate terms according to

$$\Delta\chi(f) = \chi_W(f) + \chi_{IW}(f) + \Delta\chi_I(f), \quad (9)$$

$$\chi_W(f) = \phi_W(0) - i2\pi f \int_0^\infty e^{-2\pi i f t} \phi_W(t) dt, \quad (10)$$

$$\chi_{IW}(f) = -2 \int_0^\infty e^{-2\pi i f t} \phi_{IW}(t) dt, \quad (11)$$

$$\Delta\chi_I(f) = -\frac{i}{2\pi f} \int_0^\infty (e^{-2\pi i f t} - 1) \phi_I(t) dt, \quad (12)$$

as first shown by Caillol *et al.*²¹ in 1986. The full derivation is given in Appendix A.

B. Water hydration shells and ion-pair states

The radial distribution function $g_{\text{Na},\text{O}}(r)$ between sodium and water oxygen in Figure 1(a) and $g_{\cdot,\text{O}}(r)$ between anions and water oxygen in Figure 1(b) exhibit well-defined maxima and minima, which allows to partition solvation water into distinct solvation shells. The positions of the local minima in

the radial distributions, indicated by orange vertical dashed lines for F as an anion and by black dashed lines for Cl as an anion (Br and I give positions very similar to Cl and are therefore not shown), allow to distinguish first solvation-shell water, W1, and second solvation-shell water, W2, from third solvation-shell water, W3, as indicated in the figures. Note that the shell denoted by W3 contains all water molecules that are not part of the first and second solvation shells.

Likewise, the oscillations in the sodium-anion radial distribution functions $g_{\text{Na}_a^-}(r)$ in Figure 1(c) point to distinct ion-pair configurations.^{22,23} We indicate the first three minima of $g_{\text{Na}_a^-}(r)$ by vertical dashed lines, orange for NaF and black for NaCl, the positions of the minima for NaBr and NaI are again very close to the ones for NaCl and not shown. This gives rise to four different ion-pair populations, namely, contact ion pairs (CIP), single solvent-separated ion pairs (SIP), doubly solvent-separated ion pairs (DSIP), and free ions (FI), as indicated in Figure 1(c). A schematic illustration of different ion-pair configurations is shown in Figure 1(d). The CIP lifetime is estimated as 12.3 ps for 1 M NaCl in Appendix C.

In contrast to the radial distribution functions in Figure 1(c), the number fraction n_1^k of different ion-pair configurations in Figure 1(e) is dominated by single solvent-separated ion pairs for all studied salts (here, the index k numbers the four different ion-pair states CIP, SIP, DSIP, and FI). This reflects that although for the salts NaCl, NaBr, NaI the

sodium-anion radial distribution in Figure 1(c) is maximal for CIP, the solvent-separated ion pair population wins by numbers because of the larger shell radius. Note that in determining the number fractions n_1^k the ion-pair state k of an ion is defined by the closest counterion. Also, the sum of n_1^k is normalized to unity, $\sum_k n_1^k = 1$. The most pronounced variation among different salts at 1 M is seen for the CIP, which are maximal for NaCl and almost non-existent for NaF, which reflects the strongly bound water solvation shell for NaF. When comparing the fractions n_1^k for the different concentrations of NaCl, we see that with increasing concentration the number of FI goes down while the CIP fraction goes up.

The number fraction of water in different solvation layers, denoted by n_W^k , we normalize with respect to the equivalent number of water molecules in pure water, $\sum_k n_W^k = N_W/N_{\text{bulk}}$. Here, N_W is the actual number of water molecules in the simulation of a salt solution while $N_{\text{bulk}} = V \rho_{\text{bulk}}$ is the equivalent number of water molecules in pure water in the same volume V and with bulk number density $\rho_{\text{bulk}} = 33.4 \text{ nm}^{-3}$. Due to the finite volume of the ions in solution and due to non-ideal mixing effects, the sum $\sum_k n_W^k$ is not equal to unity, so by dividing the spectral water contributions by n_W^k we eliminate trivial water dilution effects and can therefore extract a meaningful spectral contribution per water molecule. The running index k distinguishes first, second,

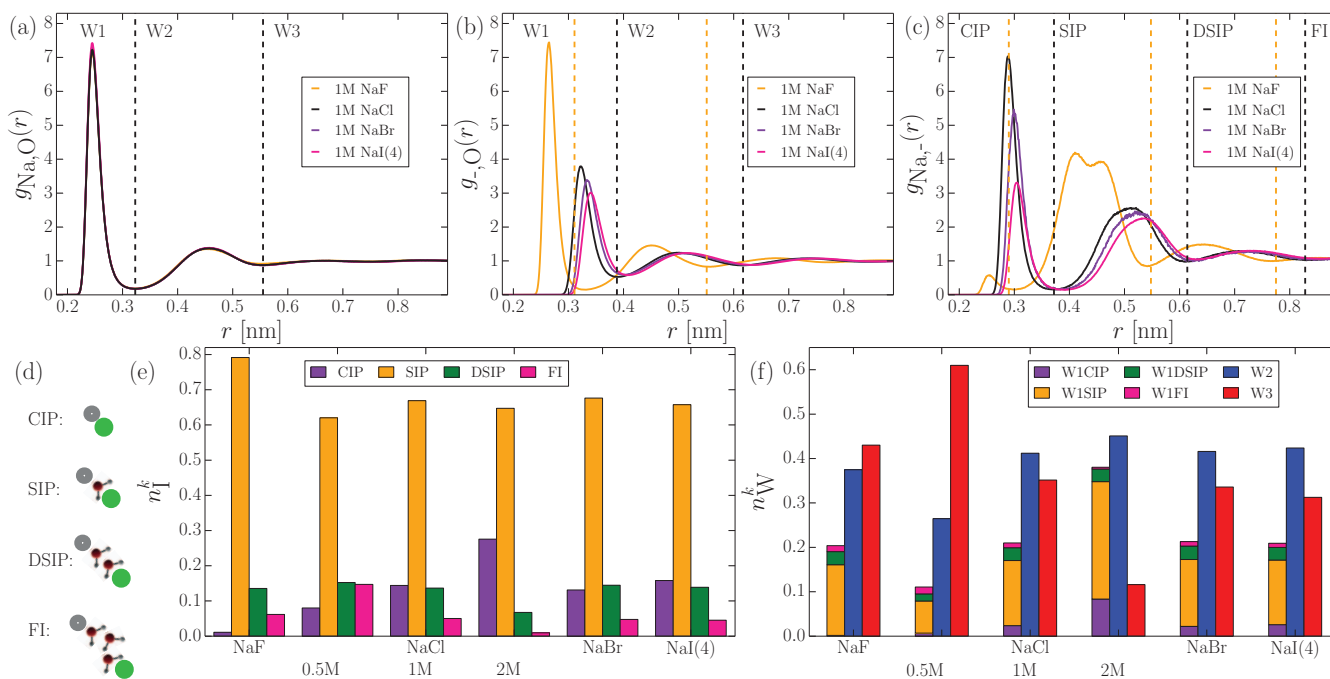


FIG. 1. Water solvation layers and ion-pair states: (a) The radial distribution functions $g_{\text{Na}_a\text{O}}(r)$ between sodium and water oxygen for the four different 1 M salt solutions NaF, NaCl, NaBr, and NaI are almost indistinguishable. The vertical dashed lines at the minima separate the 1st, 2nd, and 3rd water solvation shells. For iodide the force field I(4) is used. (b) The first maximum of the radial distribution functions $g_{a\text{O}}(r)$ between the anions and water oxygen progressively moves to smaller distances as the bare anion size decreases. The orange/black vertical dashed lines denote the minima for F and Cl, respectively, the minima for Br and I are similar to Cl and not shown. (c) The anion-cation radial distribution functions $g_{\text{Na}_a^-}(r)$ show the typical crossover from contact-ion-pairing for Cl, Br, I to solvent-separated ion pairing for F. The positions of the first three minima (denoted by vertical dashed lines) define the different ion-pair configurations as schematically indicated in (d): contact ion pairs (CIP), single solvent-separated ion pairs (SIP), doubly solvent-separated ion pairs (DSIP), and free ions (FI). The orange lines denote the minima for NaF, the black ones for NaCl, the minima for NaBr and NaI are similar to NaCl and not shown. (e) The ion-pair number fractions n_1^k , which are normalized according to $\sum_k n_1^k = 1$, are dominated by solvent-separated ion pairs (SIP) for all studied solutions. (f) Number fractions of the different solvation water components n_W^k . Note that the n_W^k components are normalized with respect to pure water and therefore $\sum_k n_W^k \neq 1$, see text. First solvation-shell water is labeled by W1 and further decomposed into the different ion-pair configurations, second and third-shell solvation water is denoted by W2 and W3, respectively.

and third (and beyond) solvation shells, in part of our analysis the first shell is further decomposed depending on the ion-pair state. Figure 1(f) shows that for 1 M solutions about 20% of the water is first solvation-shell water, and that the largest contribution to the first solvation shell comes not surprisingly from the single solvent-separated ion pairs, reflecting that these ions dominate the ion-pair fractions n_1^k shown in Figure 1(e). Note that in determining the number fractions n_W^k the state k of a water molecule is defined by the closest ion.

C. Decomposition of dielectric spectra

To analyze the different dielectric contributions of water hydration shells and ion-pair states, we decompose the polarization and current correlation functions according to

$$\phi_W^k(t) = \frac{\langle \vec{P}_W(0) \cdot \vec{P}_W^k(t) \rangle}{3Vk_B T \epsilon_0}, \quad (13)$$

$$\phi_{1W}^k(t) = \frac{1}{2} \frac{\langle \vec{P}_W(0) \cdot \vec{J}_1(t) - \vec{J}_1(0) \cdot \vec{P}_W^k(t) \rangle}{3Vk_B T \epsilon_0}, \quad (14)$$

$$\phi_1^k(t) = \frac{\langle \vec{J}_1(0) \cdot \vec{J}_1^k(t) \rangle}{3Vk_B T \epsilon_0}, \quad (15)$$

where the index k in $\phi_W^k(t)$ and $\phi_{1W}^k(t)$ stands for the previously defined different water solvation shells and in $\phi_1^k(t)$ for the different ion-pair states. Note that this decomposition is not unique, but allows to extract systematic trends and mechanistic insight in a straightforward fashion. By construction, the sums over the index k return the total correlation functions defined previously in Eqs. (3)–(5), $\phi_W(t) = \sum_k \phi_W^k(t)$, $\phi_{1W}(t) = \sum_k \phi_{1W}^k(t)$, $\phi_1(t) = \sum_k \phi_1^k(t)$.

The decomposed dielectric spectral contributions follow in analogy to Eqs. (10)–(12) as

$$\chi_W^k(f) = \phi_W^k(0) - i2\pi f \int_0^\infty e^{-2\pi i f t} \phi_W^k(t) dt, \quad (16)$$

$$\chi_{1W}^k(f) = -2 \int_0^\infty e^{-2\pi i f t} \phi_{1W}^k(t) dt, \quad (17)$$

$$\Delta \chi_1^k(f) = -\frac{i}{2\pi f} \int_0^\infty (e^{-2\pi i f t} - 1) \phi_1^k(t) dt, \quad (18)$$

and the decomposed pure ionic contributions to the conductivity are in analogy to Eq. (8) given by

$$\sigma_1^k(f) = \int_0^\infty e^{-2\pi i f t} \phi_1^k(t) dt. \quad (19)$$

Explicitly, the water dielectric contribution $\chi_W(f)$ is thus split into a total of six different terms, first into the three water solvation shells, $\chi_W(f) = \chi_{W1}(f) + \chi_{W2}(f) + \chi_{W3}(f)$, and the first-solvation-shell contribution further into the four different ion-pair contributions according to $\chi_{W1}(f) = \chi_{W1CIP}(f) + \chi_{W1SIP}(f) + \chi_{W1DSIP}(f) + \chi_{W1FI}(f)$.

D. Simulation methods

We use GROMACS 4.5.4²⁴ to simulate three separate trajectories of duration 100 ns each for the salt types NaCl, NaBr, and NaI, for bulk water only one and for NaF five trajectories are simulated. The simulation box contains about 7000 water molecules and 130 ion pairs (for the 1 M solutions) in the *NPT* ensemble at 300 K, employing the Nose-Hoover thermostat implemented in GROMACS and a 2 fs integration time step. The neighbor list is updated every 20 fs and trajectories are saved every 10 fs. Electrostatics are computed by Particle-Mesh-Ewald methods and the Lennard-Jones interactions are subject to a switch cutoff between 1.1 and 1.2 nm. We use the SPC/E water model²⁵ and our previously optimized ion force fields with non-standard mixing rules²⁶ for fluoride and iodide. Note that these ion force fields have been simultaneously optimized with respect to the single-ion solvation free energy and the activity coefficients of different ion pairs, for iodide two distinct force fields were reported that both satisfied the equilibrium optimization procedure equally well.²⁶ In the present work, we compare both force fields for iodide with experimental dielectric spectra and therefore perform an additional optimization step based on dynamic and static dielectric properties, as will be discussed further below. Because of memory limitations all trajectories are split into series of 20 ns length during data analysis. The polarization components of each time series are Fourier transformed via Fast Fourier Transformation (FFT). Correlation functions are calculated by multiplication in Fourier space according to the convolution theorem. After back transformation into the time domain the correlations are averaged over different time series. We update the decomposition of water and ions into different solvation-shell and ion-pair states every 10 fs, consequently, the ensemble of tagged molecules changes in time. Since the diffusion of ions and water molecules is slower than the polarization fluctuations, the fluctuating ensembles corresponding to different solvation shells and ion-pair states do not influence the resulting spectra and correlation functions on the frequency or time scales of interest. An upper time cutoff is imposed on the Laplace transform of the correlation functions during calculation of the spectra, as is discussed in detail in Appendix B.

III. COMPARISON WITH EXPERIMENTAL DIELECTRIC SPECTRA

In Figure 2, we compare Buchner's experimental results³ for the dielectric spectra of NaCl solutions at different concentrations with our simulation results. In Figure 2 on the left side, we reproduce the experimentally determined Cole-Cole fits to experimental data³ according to

$$\Delta \chi(f) + 1 = \frac{\epsilon_{CC} - \epsilon_\infty}{1 + (i2\pi f \tau_{CC})^{1-\alpha}} + \epsilon_\infty, \quad (20)$$

Figure 2(a) shows the real part while Figure 2(d) shows the imaginary part of the dielectric function, the latter part corresponding to the absorption spectrum. We also include the spectrum of pure water (shown in red) and plot the amplitude ϵ_{CC} and the characteristic relaxation time τ_{CC} as a function

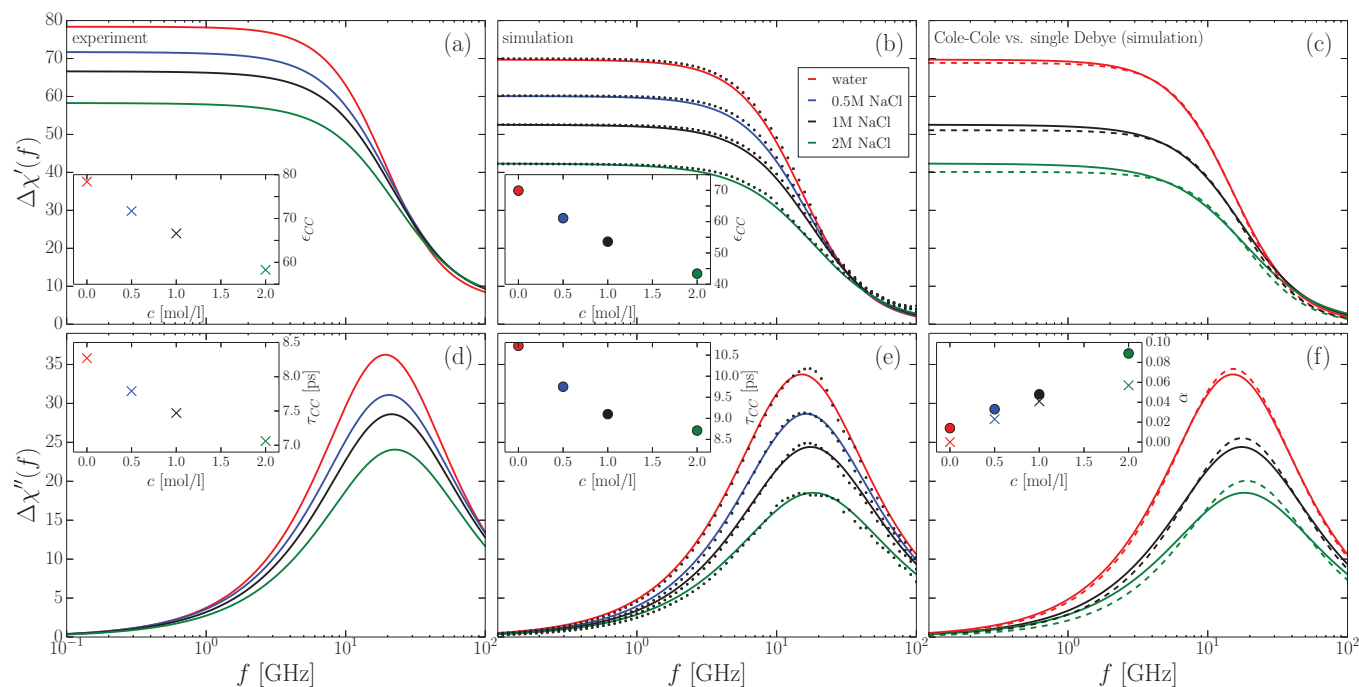


FIG. 2. Comparison of experimental and simulated dielectric spectra of NaCl solutions at matching concentrations $c = 0, 0.5, 1,$ and 2 M. (a) and (d): Experimental Cole-Cole fits of the real and imaginary parts of the dielectric susceptibility $\Delta\chi'(f)$ and $\Delta\chi''(f)$, reproduced from Buchner *et al.*³ The red lines show the results for pure water ($c = 0$ M). The dielectric constant ϵ_{CC} in the inset in (a), as obtained from the amplitude of the Cole-Cole fits, decreases as a function of NaCl concentration. The corresponding experimental relaxation time τ_{CC} in the inset in (d) exhibits a characteristic blue-shift to shorter times with rising NaCl concentration. (b) and (e) show the simulated real and imaginary parts of the dielectric susceptibility, points correspond to simulation data and lines are the Cole-Cole fits for different NaCl concentrations, including pure water (red lines). The insets again show the dielectric constant ϵ_{CC} and the relaxation time τ_{CC} as a function of NaCl concentration, which reproduce the experimental trends. (c) and (f) compare Cole-Cole fits (solid lines) and single Debye fits (dashed lines) of the simulation data. The inset in (f) shows the Cole-Cole exponent α , which is a measure of the deviations from a simple Debye form, as a function of salt concentration extracted from the experimental fits³ (crosses) and from the simulation data (filled symbols).

of concentration in the insets. Increasing salt concentration lowers the dielectric constant ϵ_{CC} , a trend that is well-known and rationalized in terms of the so called dielectric saturation effect,^{27–30} we will come back to this interpretation further below. At the same time, increasing salt concentration decreases the relaxation time and leads to a significant blue-shift, we will further below argue this shift to be mostly due to strongly bound water in the first solvation shell. In the analysis of our simulation data, we fit the real and imaginary parts of the dielectric spectrum simultaneously with the error functional $(\Delta\epsilon')^2 + (2\Delta\epsilon'')^2$ using a logarithmic distribution of sample frequencies in the range between 0.1 and 100 GHz. In order to roughly achieve the same relative errors for real and imaginary parts, we use a higher weight for the imaginary part, since it has a lower absolute value. For the simulation data, we use $\epsilon_\infty = 1$ in the Cole-Cole fitting function Eq. (20), reflecting that the used classical force field does not include atomic polarizabilities. In Figures 2(b) and 2(e), we show the real and imaginary parts of the dielectric function, dots correspond to simulation data, solid lines are Cole-Cole fits (fit parameters are listed in Table I). The fits are of very high quality, the same also holds for the decomposed spectra we present further below, so for clarity of presentation we in this paper sometimes present only the Cole-Cole fits of our simulation data. The concentration dependence of the amplitude ϵ_{CC} and the characteristic relaxation time τ_{CC} in the insets in Figures 2(b) and 2(e) show a very similar trend as the experimental data in Figures 2(a) and 2(d), namely, a decrease of both the

dielectric constant as well as the relaxation time with increasing salt concentration. While the decrement of the dielectric constant in simulations, $\epsilon_{CC} = 69.9$ for $c = 0$ mol/l to $\epsilon_{CC} = 43.4$ for $c = 2$ mol/l NaCl, is only slightly higher than in experiments, which gives $\epsilon_{CC} = 78.4$ for $c = 0$ mol/l and $\epsilon_{CC} = 58.3$ for $c = 2$ mol/l NaCl, the overall dielectric constant is lower in simulations compared to experiments. Similarly, the change of the relaxation time upon increase of salt concentration is similar in simulations compared to experiments, while the overall relaxation time in simulations is larger by about 2 ps compared to experiments. It transpires that the disagreement between experiments and simulations mainly reflects a

TABLE I. Cole-Cole fit parameters to our simulation spectra and the experimental spectra measured by Buchner *et al.*^{2–4}

	Simulation			Experiment ^{2–4}			
	ϵ_{CC}	τ_{CC} [ps]	α	ϵ_{CC}	τ_{CC} [ps]	α	ϵ_∞
Water	69.9	10.72	0.014	78.4	8.27	0.000	5.87
1 M NaF	56.8	9.65	0.042	67.8 ^a	8.28 ^a	0.036 ^a	4.96 ^a
0.5 M NaCl	61.1	9.75	0.030	71.7	7.79	0.023	5.65
1 M NaCl	53.6	9.10	0.047	66.6	7.47	0.041	5.65
2 M NaCl	43.4	8.71	0.085	58.3	7.06	0.057	5.65
1 M NaBr	52.6	9.23	0.058	66.6	7.55	0.032	5.64
1 M NaI(4)	51.5	9.07	0.056	65.5	7.19	0.039	5.05

^aExperimental Cole-Cole fit parameters for 0.86 M NaF were received in a private communication by R. Buchner and linearly extrapolated to 1 M.

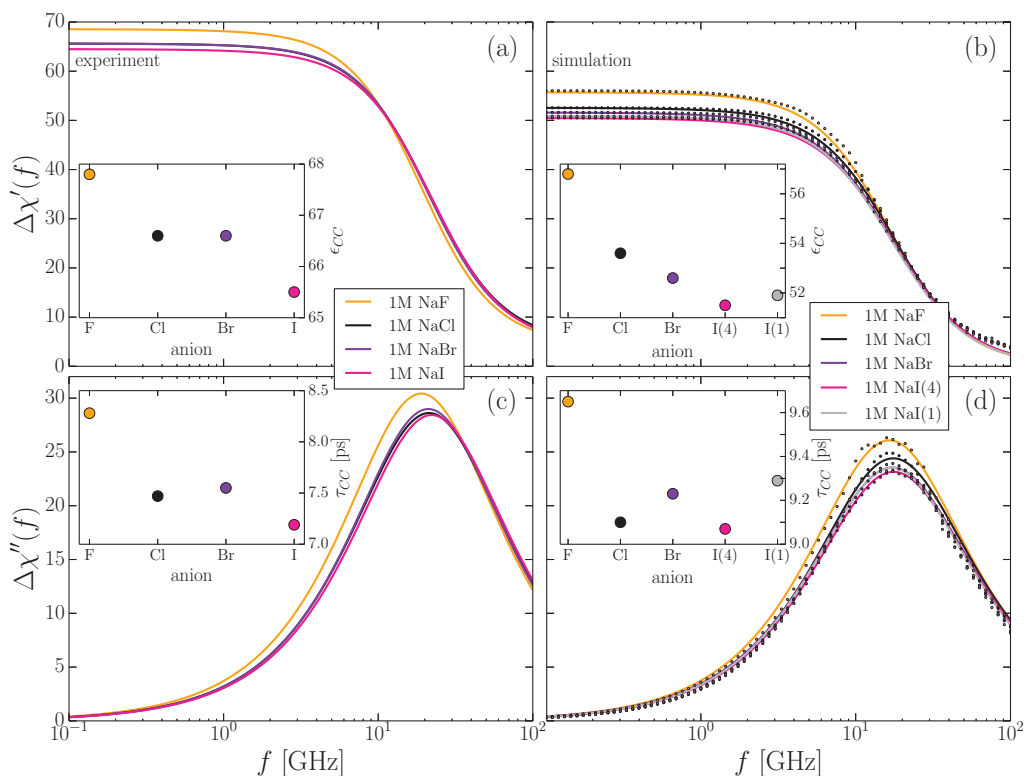


FIG. 3. Comparison of experimental and simulated dielectric spectra of NaF, NaCl, NaBr, and NaI solutions at concentration $c = 1$ M. (a) and (c) Experimental Cole-Cole fits of the real and imaginary parts of the dielectric susceptibility $\Delta\chi'(f)$ and $\Delta\chi''(f)$ for the different salt types, reproduced from Buchner *et al.*²⁻⁴ The dielectric constant ϵ_{CC} in the inset in (a), as obtained from the amplitude of the Cole-Cole fits, decreases with increasing size of the anion, with the exception of Br. The corresponding experimental relaxation time τ_{CC} in the inset in (c) shows a similar trend: Larger anions are characterized by smaller relaxation times. (b) and (d) show the simulated real and imaginary parts of the dielectric susceptibility, points correspond to simulation data and lines are Cole-Cole fits for the different salt types. The insets again show the dielectric constant ϵ_{CC} and the relaxation time τ_{CC} for the different salt types. Note that results for two different force fields for iodide are shown, the force field combination NaI(4) reproduces the experimental trends much better.

deficiency of the SPC/E water model, which is well known and amply documented in literature for the static dielectric properties.³¹⁻³³ As a side remark we note that previous simulations of NaCl solutions in SPC/E water give a somewhat better agreement of the simulated spectra with experimental data,¹¹ but it seems that this is spurious and caused by an incorrect treatment of the ion-water cross-polarization term, as we will discuss further below.

Overall, the ion-dependent changes of the simulated spectra match experimental data quite well, both the change in dielectric strength and in relaxation time are reproduced remarkably well. The simulation data (dots in Figures 2(b) and 2(e)) are well described by Cole-Cole fits, which demonstrates that the Cole-Cole fitting parameters constitute a useful set to describe simulated dielectric spectra. The deviations of the simulated data from the simple Debye form (obtained by setting $\alpha = 0$ in Eq. (20)) increase with salt concentration, this is demonstrated in Figures 2(c) and 2(f) where we compare Debye fits (broken lines) with Cole-Cole fits (solid lines). The inset of Figure 2(f) shows the Cole-Cole exponent α as a function of salt concentration, where circles denote simulation and crosses experimental results, α quantifies spectral deviations from the Debye form. We see that while pure water in simulations shows almost Debye-type dielectric relaxation, characterized by $\alpha = 0.014$, the higher concentrated NaCl solutions exhibit significantly larger α values and thus pronounced deviations from simple Debye relaxation. A

naïve interpretation would be that the deviations from simple Debye-type relaxation are caused by the superposition of water and ionic relaxation processes at different relaxation frequencies, our decomposition analysis demonstrates that this naïve interpretation is not in agreement with a more detailed analysis of the data.

To study ion specific effects on the dielectric relaxation, we in addition simulated NaF, NaBr, and NaI solutions at fixed concentration $c = 1$ M. In Figure 3 (left side), we show the matching experimental Cole-Cole fits reproduced from Buchner *et al.*²⁻⁴ for the (a) real part and the (c) imaginary part of the dielectric function. The experimental data show a clear ion-specific trend, NaF (orange lines) has the strongest and NaI (pink lines) the weakest dielectric signal, which is most clearly presented in the inset of Figure 3(a) where we plot the dielectric constant ϵ_{CC} for the four different salt types. A similar ion-specific trend is observed for the relaxation time τ_{CC} which is plotted in the inset of Figure 3(c), the smallest anion F leads to the longest relaxation while the largest anion I gives rise to the fastest relaxation. The simulation data in Figures 3(b) and 3(d) exhibit very similar behavior, except an offset the dielectric constant ϵ_{CC} in the inset of Figure 3(b) and the relaxation time τ_{CC} in the inset of Figure 3(d) reproduce the experimental trends very well. The offsets are similar to the data for pure water shown in Figure 2, so similar to our discussion of the salt-concentration dependent data above, we conclude that the disagreement between experimental and

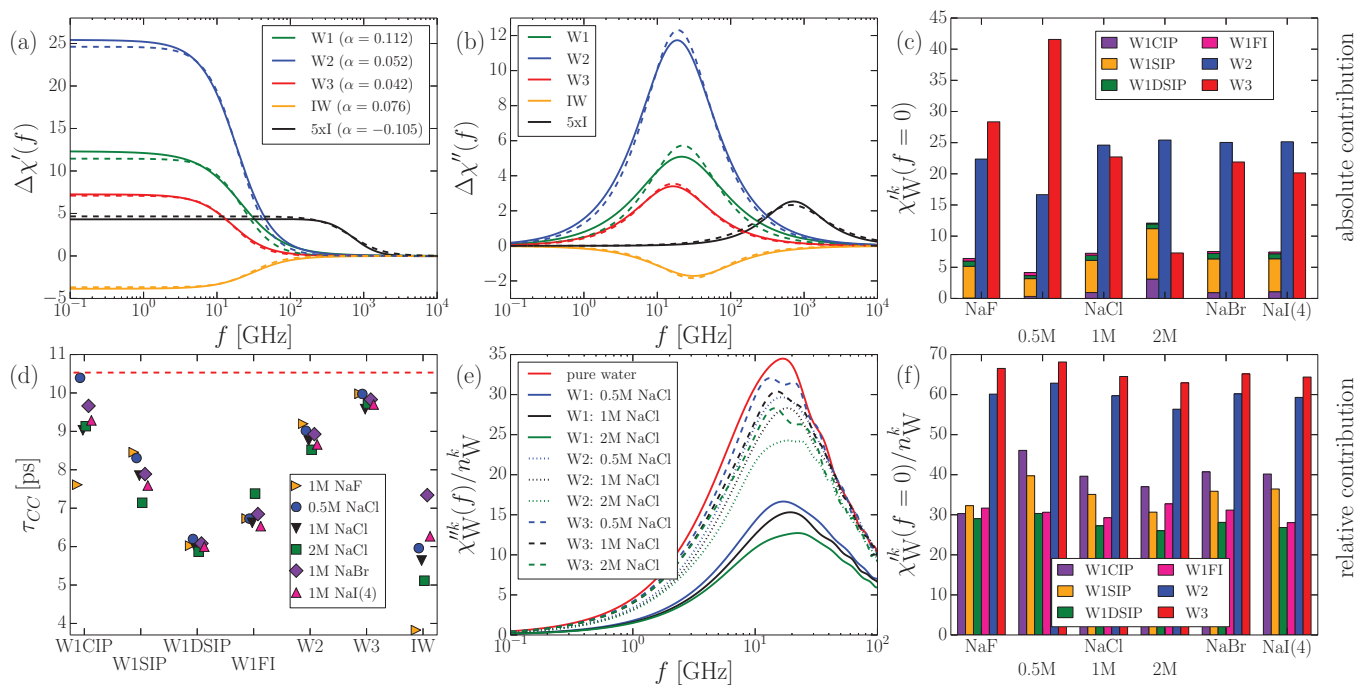


FIG. 4. Simulation results for the decomposition of dielectric spectra. (a)+(b) Decomposition of the real and imaginary parts of $\Delta\chi(f)$ for 2 M NaCl into contributions from the first water solvation shell W1 (green), second shell W2 (blue), third shell W3 (red), ion-water cross-contribution (IW, orange), and the ionic contribution (I, black, increased by a factor of five for better visibility). Dashed lines denote single Debye fits and solid lines are Cole-Cole fits. (c) Absolute contribution of the different water shells to the static dielectric constant for all different solutions. (d) Dielectric relaxation time τ_{CC} of the different water shells for all salt solutions, obtained from Cole-Cole fits. The horizontal red dashed line denotes the bulk water dielectric relaxation time. (e) Imaginary dielectric function per water molecule for different water solvation shells, $\chi_{W^k}^{kk}(f)/n_{W^k}^k$, for NaCl at different concentrations: The first solvation shell (W1, solid lines) has the weakest contribution of only about 50% of pure water (red line). (f) Relative contribution of the different water shells to the static dielectric constant for all different salt solutions $\chi_{W^k}^{kk}(f=0)/n_{W^k}^k$.

simulation data for the different ions is mostly caused by deficiencies of the water model. Note that the static dielectric constants we obtain in our simulations are slightly lower than obtained indirectly from ionic distribution functions in earlier work.²²

In our simulations, we use two distinct force fields for iodide, the results are slightly different and denoted by NaI(4) and NaI(1) in Figures 3(b) and 3(d). These force fields were found to be of equal quality in our previous ion force-field optimization studies based on the simultaneous matching of experimental single-ion solvation free energies and activity coefficients,²⁶ in other words, the two iodide force fields are degenerate with respect to the static properties employed in our optimization. A comparison of the simulated and experimental dielectric constants ϵ_{CC} and relaxation times τ_{CC} in the insets of Figure 3 show that force field I(4) performs significantly better compared to force field I(1). We conclude that based on the combined static and dynamic experimental data for dielectric relaxation times, dielectric constants, single-ion solvation free energies, and activity coefficients force field I(4) is superior to force field I(1), including dielectric properties thus lifts the degeneracy of the two iodide force fields. Our force fields even reproduce the weak irregularity of bromide, which experimentally has a slightly larger relaxation time than both chloride and iodide, see Figures 3(c) and 3(d). This might be interpreted in favor of the force fields used by us in the present study, though we hasten to add that for the dielectric constant our simulation data for Br do not reproduce the sim-

ilar irregularity in the experimental data, see Figures 3(a) and 3(b).

All in all we conclude that the simulation data reproduce the ion-specific trends of the dielectric relaxation spectra in a remarkably accurate fashion, which serves as a validation of both our force fields and the simulation technology, and therefore warrants our more detailed ion-specific analysis of the water and ion relaxation contributions.

IV. SEPARATE DIELECTRIC SPECTRA FOR WATER AND IONS

In Figures 4(a) and 4(b), we show the spectral decomposition of the real and imaginary dielectric functions for 2 M NaCl into the contributions from the three solvation shells, W1, W2, and W3, the ion-water cross term (IW) and the ion-ion term (I), note that the latter contribution is multiplied by a factor of five for better visibility. Solid lines show Cole-Cole fits and dashed lines show single Debye fits to our simulation data. The sum of all five contributions reproduces the full dielectric spectrum shown previously in Figures 2(b) and 2(e) according to $\Delta\chi(f) = \chi_{W1}(f) + \chi_{W2}(f) + \chi_{W3}(f) + \chi_{IW}(f) + \Delta\chi_I(f)$. Most strikingly, the spectrum is dominated by the second solvation shell water contribution (W2, blue line), followed by first (W1, green line), and third shell (W3, red line) contributions. The ion-water cross contribution (IW, yellow line) is negative and therefore significantly weakens the total dielectric response. This cross term has been controversially discussed in literature and can be interpreted as an ionic

screening effect on the water dielectric function (see Ref. 5 for a discussion and a detailed list of references). In fact, it seems that in earlier simulation work on NaCl solutions the ion-water cross term had the incorrect sign, giving rise to a positive contribution to the total spectrum.^{5,6,11} Although this would spuriously improve the agreement of the total spectrum with experiments, the correct sign used in previous^{7,13} and in the present work attenuates the dielectric response of water which is in line with an interpretation in terms of ions screening and thus weakening the water dielectric response (see Appendix A for an explicit derivation of the various dielectric contributions).

The Cole-Cole exponent for the five contributions in the legend in Figure 4(a) has for the given first-solvation shell water contribution W1 the value $\alpha = 0.112$, which is larger than the value for the total spectrum for 2 M NaCl $\alpha = 0.085$ shown in Figure 2(f). Indeed, while the Cole-Cole and single-Debye fits (solid and broken lines in Figures 4(a) and 4(b)) for the third-solvation shell water (W3, red lines) agree quite well, in line with a rather small exponent $\alpha = 0.042$, the two fitting forms show increasing deviations as one goes to the inner solvation shells. Therefore, an interpretation of the non-Debye like character of the dielectric response of salt solutions as being caused by the addition of two distinct processes caused by ion and water relaxation that are each Debye-like but occur at different relaxation times is not in line with our results: Rather, our decomposition into ion, ion-water, and different water-solvation shell contributions reveals that deviations from a single Debye form are caused by the intrinsic non-Debye-like character of the strongly bound solvation water in the first solvation shell around ions. This conclusion is supported by the fact that the relaxation times of the dominant dielectric contributions in Figure 4(b) are quite similar. In Appendix D, we demonstrate that a further decomposition of the first solvation-shell water into sub-contributions for distinct ion-pair configurations does not make the individual processes more Debye-like, lending even more weight to this conclusion. The increase of the Cole-Cole exponent α in Figure 2(f) from $\alpha = 0.014$ for $c = 0$ M to $\alpha = 0.085$ for $c = 2$ M can therefore partly be traced back to the increase of the fraction of inner shell water n_{W1} with concentration (see Figure 1(f)), which is characterized by a significantly higher $\alpha = 0.112$ value compared to the other solvation layers.

The absolute contribution of the different solvation-water shells $\chi_W^k(f=0)$ to the total static dielectric constant for all studied solutions is shown in Figure 4(c). This plot mostly reflects the different numbers of water molecules in the different solvation layers. More meaningful is the relative contribution $\chi_W^k(f=0)/n_W^k$ in Figure 4(f), where we rescale $\chi_W^k(f=0)$ by the water number fraction n_W^k . Here, it is seen that the relative contribution for third shell water $\chi_{W3}^k(f=0)/n_{W3}^k$ is close to the bulk water value of about 70, while for second-shell water $\chi_{W2}^k(f=0)/n_{W2}^k$ is reduced by about 15% and for first-shell water $\chi_{W1}^k(f=0)/n_{W1}^k$ the relative contribution is only about half of the bulk value (note that for first-shell water we further decompose into the different ion-pair states). Since by construction the various dielectric contributions are additive, we conclude that the dielectric saturation effect in salt solutions is (apart from a trivial dilution effect because of

the finite ionic volume) mainly caused by the reduction of the dielectric amplitude in the first water solvation shell around ions.

There are two distinct explanations for the dielectric decrement in salt solutions, keeping in mind that the dielectric spectrum is dominated by the water contributions and therefore also the decrement must be related to how water reacts to the presence of ions in the solution: The first explanation rationalizes the decrease of the water polarizability by water orientation in the ionic electric fields, a mechanism usually called dielectric saturation. This explanation neglects correlations between water molecules and rather invokes a single-dipole picture: Clearly, in an orienting electric field, the polarizability of a single dipole decreases. The second explanation is less intuitive but explicitly considers the effect of correlations between water molecules on the dielectric response. According to the Madden-Kivelson-theory,³⁴ the Kirkwood factor g_K , which is the dielectric enhancement factor due to correlations between water molecules,³⁵ is linearly related to the relaxation time. For water g_K is known to be high and of the order of $g_K \simeq 2.3$,³⁶ so a decrease of the dielectric contribution of the first solvation shell can alternatively be interpreted as being caused by a loss of correlations between water molecules. This interpretation is reasonable in light of the perturbing influence of an ion on the local water structure. To obtain further evidence for this decorrelation effect, we in Figure 4(d) show the relaxation times τ_{CC} of all individual water solvation shells for all studied salt solutions. Different salts and different concentrations for NaCl show quite similar behavior and a clear trend: Third solvation shell water W_3 has a relaxation time similar to bulk water (shown as a broken horizontal line), the second shell water W_2 has a substantially reduced relaxation time, and the relaxation time of water in the first solvation shell (except around contact-ion-pair ions W1CIP) is even further reduced. This decomposition therefore demonstrates that the blue shift of the dielectric spectra of salt solutions mainly comes from a blue shift of first-solvation water shell. Note that the relaxation time of first-solvation shell water progressively increases for ions that are bound to each other more closely, i.e., as one goes from doubly solvent separated ion pairs (WIDSIP) over solvent-separated ion pairs (WISIP) to contact ion pairs (W1CIP). This trend correlates very nicely with the results for the dielectric constant per water molecule for the different water solvation types in Figure 4(f). Our data thus show a good correlation between relaxation times and dielectric constants for the different water solvation layers in qualitative agreement with the Madden-Kivelson-theory originally derived for homogeneous liquids, we thus conclude that the dielectric decrement observed in salt solutions is in line with a decorrelation mechanism of water in the first and also in the second solvation shell around ions. We note that this does not rule out that also dielectric saturation plays a role in our systems, because the relaxation time of a single dipole in a strong external electric field is also expected to go down. But since correlation effects are dominant for liquid water, as witnessed by the large Kirkwood factor of $g_K \simeq 2.3$ in bulk water, we argue that a single dipole picture is not applicable in order to understand the dielectric decrement in salt solutions.

In Figure 4(e), we plot the imaginary dielectric function per water molecule $\chi_W^{ik}(f=0)/n_W^k$ for the three water solvation shells W1, W2, and W3 for NaCl at the three different concentrations $c = 0.5, 1, 2$ M and compare with the corresponding result for pure water (red solid line). We see that the spectral contribution of the third solvation shell W3 is almost bulk-like, while distinct deviations are discerned for W2. The spectrum of the first solvation shell W1 (solid lines) is reduced to about half the bulk value and the blue shift, which is more clearly seen in Figure 4(d), can already be discerned. Interestingly, the outer shell spectra W2 and W3 converge to the bulk curve for high frequencies, meaning that deviations between bulk and solvation water mostly concerns slow, low-frequency processes.

A decomposition of experimental spectra into three single Debye processes often leads to a slow ionic, a dominant bulk water-like, and fast water process with relaxation times separated by more than one order of magnitude.⁴ In our simulations, the differences are smaller, since the fastest inner shell water (WIDSIP) is only about a factor of two faster than bulk water, as seen in Figure 4(d).

A. Detailed analysis of ion-water cross correlations

The ion-water dielectric cross-correlation function $\phi_{IW}(t)$ in Figure 5(a) shows a steep initial decay over roughly 1 ps

followed by a much slower relaxation. $\phi_{IW}(t)$ is odd in time, as seen more clearly in the inset, and positive for all studied solutions, reflecting that $P_W(0)J_1(t)$ is larger than $J_1(0)P_W(t)$, see Eq. (4). This is in accord with previous simulation results for various ionic liquids^{9,10} except 1-ethyl-3-methylimidazolium triflat (EMIM⁺CF₃SO₃⁻), where an opposite time-correlation has been reported.¹² We have reliable data for $\phi_{IW}(t)$ up to about 10 ps; this allows to calculate the spectral contribution $\chi_{IW}(f)$ in Figure 5(b), which is characterized by a relaxation time around $\tau_{IW} \simeq 5$ ps about a factor two faster than bulk water. We see pronounced ion specific trends in the short time behavior of $\phi_{IW}(t)$ (inset of Figure 5(a)), for the smallest anion fluoride $\phi_{IW}(t)$ displays a maximum at the shortest time and – comparing only the 1 M solutions – has the highest amplitude and the fastest decrease. With increasing anion size the maximum is shifted to longer times. This translates into the ionic specific series of the real zero-frequency contribution $\chi_{IW}'(f=0)$ shown in the inset of Figure 5(b).

By splitting up the ion-water cross-term $\phi_{IW}(t)$ into the different water shells for 1 M NaCl in Figure 5(c) we see that the correlation between ions and first-solvation shell water IW1 dominates at the shortest time scales (as comes out from the inset), while correlations with second-solvation shell water IW2 dominate at longer times scales. Consequently, the amplitude of the spectral contribution of the ion cross-correlations with the second shell $\chi_{IW2}(f)$ exceeds

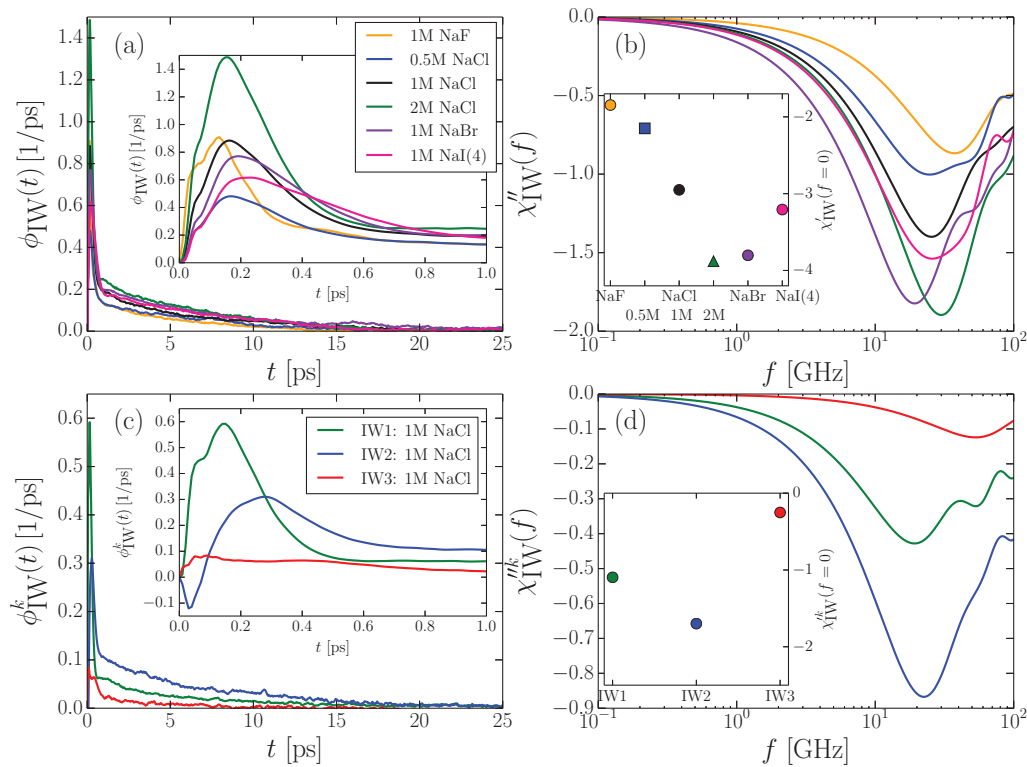


FIG. 5. Detailed analysis of ion-water cross correlations: (a) The ion-water cross-correlation function $\phi_{IW}(t)$ exhibits a fast drop over less than a picosecond followed by a much slower decrease. The inset shows the short-time behavior and demonstrates that $\phi_{IW}(t)$ is antisymmetric for all studied salt solutions. (b) Imaginary part of the ion-water dielectric contribution $\chi_{IW}''(f)$ for all studied salts. The inset shows the static real dielectric contribution $\chi_{IW}'(f=0)$. Real as well as imaginary parts are negative and thus decrease the total dielectric response function. (c) Ion-current cross correlation functions $\phi_{IW}^k(t)$ for different water shells for 1 M NaCl. The inset shows the short-time behavior and demonstrates that the first shell (green line) reaches its maximum at a shorter time compared to the second shell (blue line), while the third shell (red line) shows only negligible correlations. (d) Imaginary dielectric spectra $\chi_{IW}^k''(f)$ for different water shells for 1 M NaCl. The inset shows the static real dielectric contribution $\chi_{IW}^k'(f=0)$. The second-shell contribution IW2 dominates the frequency-dependent response function.

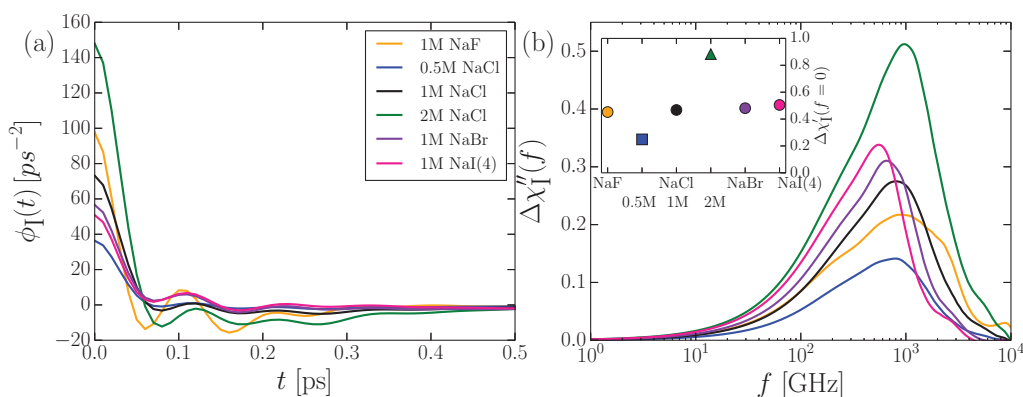


FIG. 6. Detailed analysis of ion-ion correlations: (a) Ion auto-correlation functions $\phi_1(t)$ for all studied salt solutions. $\phi_1(t)$ exhibits pronounced oscillations and decreases quickly within a few hundred fs. (b) Imaginary DC-conductivity corrected dielectric ion contribution $\Delta\chi_1''(f)$ for all different salt types. The inset shows the static real contribution $\Delta\chi_1'(f=0)$. For the 1 M solutions, the ion part $\Delta\chi_1(f)$ contributes only about 1% to the total dielectric signal and can thus be neglected for all practical purposes.

$\chi_{IW1}(f)$, as shown in Figure 5(d) for the imaginary part of the spectrum as well as for the static limit in the inset. The correlation between ions and third solvation shell water is weak and largely irrelevant. The spectral contribution of the water-ion cross-term is commonly denoted as kinetic dielectric decrement. A recent non-equilibrium study of aqueous NaCl solutions shows that the absolute value of the static decrement of the ion-water contribution does not increase monotonically with increasing salt concentration. Instead, the maximum value occurs at a salt concentration of about 2 M.³⁷ In our simulations, the second solvation shell water contributes stronger to the static decrement than the first shell. Clearly, at very high concentrations most of the water will be in the first shell and only a minor part will be in the strongly contributing second shell. Therefore, the loss of second shell water might explain the smaller absolute value of the decrement at very high concentrations.

B. Analysis of ion-ion correlations and frequency-dependent conductivity

The auto-correlation function of the ion-current, $\phi_1(t)$, shown in Figure 6(a) for all different salt types and salt concentrations, exhibits high-frequency oscillations and decreases quickly within a few hundred fs for all different salt solutions. Figures 4(a) and 4(b) demonstrate that the ion contribution $\chi_1(f)$ is the weakest of the three main contributions to the dielectric susceptibility $\chi_w(f)$, $\chi_{IW}(f)$, and $\chi_1(f)$, and accordingly has not been included in earlier simulation studies of aqueous NaCl solutions.^{6,7,11} We recall that the DC-conductivity correction only effects the imaginary part of $\Delta\chi_1(f)$, leading to a vanishing $\Delta\chi_1''(f)$ in the low frequency limit. As shown in Figure 6(b), $\Delta\chi_1''(f)$ is peaked around 1 THz, the maximum shifts to lower frequencies with increasing anion size (this is most clearly seen when comparing the different salt solution data at 1 M). In contrast to our findings that the ionic process is much faster than bulk water, a slow process in the sub-GHz range appearing in experimental spectra is often interpreted as an ionic contribution.^{2,4} Within the limited accuracy of our data for $\phi_1(t)$, which is particularly prone to numerical errors (see Appendix B 3 for

an in-depth discussion) and only allows us to sample fast relaxations, we cannot say whether a slow ionic process exists or not. In our simulations, the spectral contribution $\Delta\chi_1''(f)$ shows a red-shift as the anion size increases, which simply reflects that larger ions move more slowly through water. The real part $\Delta\chi_1'(f=0)$ amounts to a positive contribution to the total static dielectric constant of only about 1% for 1 M salt solutions, see the inset in Figure 6(b). Interestingly, the static dielectric contribution from ion positional fluctuations $\Delta\chi_1(f=0)$ scales roughly linearly with the salt concentration for NaCl, which indicates that it is due to uncorrelated and random ion positional fluctuations.

The frequency-dependent ionic conductivity $\sigma(f)$ is defined as the electric current response of free ionic charges to an external electric field and directly observable in simulations. According to Eq. (6), $\sigma(f)$ has two contributions, the first due to ion current self-correlations, $\sigma_1(f)$, and the second due to cross correlations between the ion current and the water polarization, $\sigma_{IW}(f)$. Figures 7(a) and 7(b) show our results for the frequency dependent real and imaginary parts of $\sigma(f)$ for all studied salt solutions, the results for NaCl are in good agreement with earlier studies.¹¹ There are obvious and trivial differences between the NaCl results for different salt concentrations, larger salt concentrations lead to higher conductivities at all frequencies, but no clear and systematic ion-specific trends can be discerned when comparing the spectra for different salts at equal concentration of 1 M. Only the static conductivity $\sigma_0 = \sigma(f=0) = \sigma_1(f=0)$ is directly observable in experiments, in fact, our simulation results for the molar conductance σ_0/c (black bars in Figure 7(c)) are in fairly good agreement with experimental values²⁻⁴ (blue bars in Figure 7(c)) for all different salt types and salt concentrations. In Figure 7(c), we also show the conductance $\sigma_0^k/(c n_1^k)$ for the different ion-pair configurations CIP, SIP, DSIP, and FI, each properly normalized by the fraction of the different ion-pair configurations in solution n_1^k . We see, not surprisingly, that free ions FI exhibit the largest conductance, DSIP, and SIP show a reduced conductance, and CIP ions have a conductance that is typically reduced by more than a factor of two. Note that ion pairs contribute to the conductance by rotation and by small changes in the ion separation.

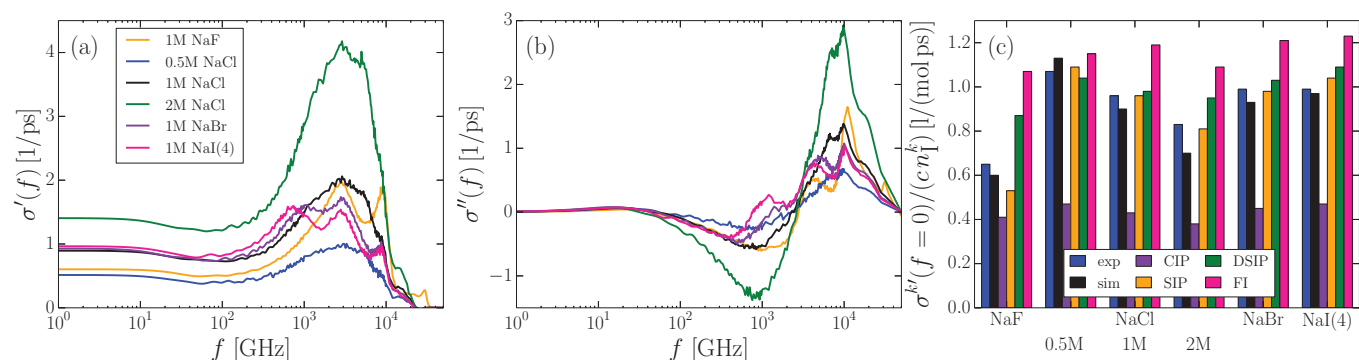


FIG. 7. Analysis of the frequency dependent conductivity. (a) Real and (b) imaginary parts of the ionic conductivity $\sigma(f)$ of all studied salts. (c) Comparison of the total static conductance $\sigma(f=0)/c$ from simulations (black bars) and from experimental data²⁻⁴ (blue bars) is favorable for all different salt solutions. The molar conductances $\sigma^k(f=0)/(cn_1^k)$ of different ion-pair configurations demonstrate that contact ion pairs (CIP) have a significantly reduced conductance compared to free ions (FI), doubly solvent-separated ion pairs (DSIP), and single solvent-separated ion pairs (SIP) only show a weakly reduced conductance (except for fluoride, where also the SIP conductance is considerably reduced).

The experimental molar conductance of NaCl solutions decreases from infinite dilution to the saturating concentration by more than a factor of two.³⁸ Our decomposition into the conductances of different ion-pair contributions allows to shed new light on the concentration dependence of the total conductance of salt solutions. For this we write the total conductance $\sigma_0(c)/c$ as the sum of the conductances $\sigma_0^k/(cn_1^k)$ of different ion-pair configurations according to

$$\frac{\sigma_0(c)}{c} = n_1^{\text{CIP}} \frac{\sigma_0^{\text{CIP}}}{cn_1^{\text{CIP}}} + n_1^{\text{SIP}} \frac{\sigma_0^{\text{SIP}}}{cn_1^{\text{SIP}}} + n_1^{\text{DSIP}} \frac{\sigma_0^{\text{DSIP}}}{cn_1^{\text{DSIP}}} + n_1^{\text{FI}} \frac{\sigma_0^{\text{FI}}}{cn_1^{\text{FI}}},$$

note that both σ_0^k and n_1^k are of course concentration dependent. For NaCl, the simulated total molar conductance (black bars in Figure 7(c)) decreases from $c = 0.5$ M to $c = 2$ M by 38%, in contrast, the molar conductance of individual ion-pair configurations shows a much weaker concentration dependence, the largest decrease of $\sigma_0^k/(cn_1^k)$ we observe for SIP for which the molar conductance decreases by 26% when going from $c = 0.5$ M to $c = 2$ M. We conclude that a significant part of the molar conductance decrement as salt concentration increases comes from the growing weight n_1^{CIP} of the weakly conducting contact-ion pairs and the reversely decreasing weight n_1^{FI} of the highly conducting free ions, see Figure 1(e). Note that our reasoning breaks down at low concentrations, where long-ranged Coulombic interactions lead to a universal reduction of the conductance of free ions that scales as the square root of the salt concentration.³⁹ Rather, our findings explain the molar conductance reduction seen at larger concentrations above 100 mM in terms of the progressive replacement of highly conducting ion-pair configurations by weakly conducting ion-pair configurations.

V. CONCLUSIONS

From the good agreement between the experimental and simulated dielectric spectra, we conclude that the halide force fields that were optimized based on thermodynamic properties²⁶ reproduce the ion specific dielectric effects quite well, this is in particular noteworthy for the dielectric relaxation time, which comes out naturally in good agreement with

experimental data. The two force fields used for iodide, denoted by NaI(4) and NaI(1), were found to be of equal quality in our previous ion force-field optimization studies.²⁶ This degeneracy of the two iodide force fields could be lifted by the comparison of the simulated and experimental dielectric constants ϵ_{CC} and relaxation times τ_{CC} in the insets of Figures 3(b) and 3(d). This shows that dielectric properties can very well be used to optimize ionic force fields.

Due to improved simulation statistics and the correct treatment of the ion-water cross-correlation polarization term we show that this term is negative and considerably suppresses the total dielectric response. We also analyze the ion autocorrelation polarization contribution and show that it contributes only about 1% to the static dielectric constant. The decomposition of the dominant water polarization contribution into different solvation shells demonstrates that the first solvation shell shows the strongest ionic influence and is predominantly responsible for the blue shift and the dielectric decrement of the total dielectric spectra. By a further decomposition of the first water solvation shell into different ion-pair states we show that the static conductance of contact ion pairs is more than 50% lower than for the other ion pairs, this partly explains the reduced conductance of concentrated salt solutions.

Our spectral decomposition suggests that the non-Debye-like character of salt solution spectra is not due to the superposition of different elementary relaxation processes with different relaxation times but rather an inherent spectral signature of the first solvation shell of water around ions. It would be interesting to investigate whether a different decomposition of the dielectric contribution from the first solvation shell into separate Debye processes is possible.

Although the experimental salt-concentration dependent and ion-specific trends of the dielectric constant and the dielectric relaxation time are well reproduced by our simulations, the absolute values are off, which we rationalize by a deficiency of the SPC/E water model we use. In the future, it would be crucial to redo the present simulations with a water model that reproduces the experimental dielectric properties of pure water, unfortunately the ion force fields would most likely have to be re-optimized for such a water model.

ACKNOWLEDGMENTS

We thank R. Buchner for discussions and for supplying additional unpublished data. We gratefully acknowledge financial support from the DFG via SFB 1078 and computing time on the HPC cluster at ZEDAT, Freie Universität Berlin. S.G. thanks the Volkswagen Foundation for financial support.

APPENDIX A: RELATION BETWEEN DIELECTRIC FUNCTIONS AND POLARIZATION CORRELATION FUNCTIONS

The derivation closely follows Caillol *et al.*²¹ Starting point is the defining relation for the electric susceptibility $\chi(f)$ relating the polarization $\vec{P}(f) = \chi(f)\epsilon_0\vec{E}(f)$ with the electric field \vec{E} (vector arrows are skipped for clarity in the following derivation),

$$\begin{aligned}\chi(f) &= \frac{1}{3Vk_B T \epsilon_0} \int_0^\infty e^{-2\pi i f t} \langle P(0) \dot{P}(-t) \rangle dt \\ &= -\frac{1}{3Vk_B T \epsilon_0} \int_0^\infty e^{-2\pi i f t} \langle P(0) \dot{P}(t) \rangle dt, \quad (\text{A1})\end{aligned}$$

where we have used $P(0)\dot{P}(-t) = -P(0)\dot{P}(t)$, since $\dot{P}(t)$ is antisymmetric and $P(t)$ is symmetric under time-reversal. In a salt solution, the total polarization $P(t) = P_W(t) + P_I(t)$ has two parts: The first part $P_W(t)$ is the total polarization of the water molecules, which poses no problems in a simulation employing periodic boundary conditions. The total polarization of the ion distribution however depends on the position of the bounding box and gives rise to spurious effects when ions traverse the simulation box boundaries. Therefore, we use the ionic current $J_I(t) = \dot{P}_I(t)$ instead,

$$\begin{aligned}\chi(f) &= -\frac{1}{3Vk_B T \epsilon_0} \int_0^\infty e^{-i2\pi f t} \langle (P_W(0) \\ &\quad + P_I(0))(\dot{P}_W(t) + J_I(t)) \rangle dt \quad (\text{A2})\end{aligned}$$

which can be split into three contributions according to $\chi(f) = \chi_W(f) + \chi_{IW}(f) + \chi_I(f)$. We obtain

$$\chi_W(f) = -\frac{1}{3Vk_B T \epsilon_0} \int_0^\infty e^{-2\pi i f t} \langle P_W(0) \dot{P}_W(t) \rangle dt \quad (\text{A3})$$

$$\begin{aligned}&= \frac{1}{3Vk_B T \epsilon_0} \left[\langle P_W^2(0) \rangle \right. \\ &\quad \left. - i2\pi f \int_0^\infty e^{-2\pi i f t} \langle P_W(0) P_W(t) \rangle dt \right] \quad (\text{A4})\end{aligned}$$

$$= \phi_W(0) - i2\pi f \int_0^\infty e^{-2\pi i f t} \phi_W(t) dt, \quad (\text{A5})$$

$$\begin{aligned}\chi_{IW}(f) &= -\frac{1}{3Vk_B T \epsilon_0} \int_0^\infty e^{-2\pi i f t} \langle P_W(0) \dot{P}_I(t) + P_I(0) \dot{P}_W(t) \rangle dt \\ &= \frac{1}{3Vk_B T \epsilon_0} \left[2\langle P_W(0) P_I(0) \rangle \right. \\ &\quad \left. + \int_0^\infty \langle P_W(0) P_I(t) + P_I(0) P_W(t) \rangle \frac{d}{dt} (e^{-2\pi i f t}) dt \right] \quad (\text{A6})\end{aligned}$$

$$\begin{aligned}&= \frac{1}{3Vk_B T \epsilon_0} \left[2\langle P_W(0) P_I(0) \rangle \right. \\ &\quad \left. + 2 \int_0^\infty \langle P_W(0) P_I(t) \rangle \frac{d}{dt} (e^{-2\pi i f t}) dt \right] \quad (\text{A7})\end{aligned}$$

$$= -\frac{2}{3Vk_B T \epsilon_0} \int_0^\infty e^{-2\pi i f t} \langle P_W(0) J_I(t) \rangle dt \quad (\text{A8})$$

$$= -2 \int_0^\infty e^{-2\pi i f t} \phi_{IW}(t) dt, \quad (\text{A9})$$

where we used that $P_W(0)P_I(t)$ is even under time-reversal in Eq. (A7),

$$\chi_I(f) = -\frac{1}{3Vk_B T \epsilon_0} \int_0^\infty e^{-2\pi i f t} \langle P_I(0) J_I(t) \rangle dt \quad (\text{A10})$$

$$= \frac{1}{3Vk_B T \epsilon_0} \int_0^\infty e^{-2\pi i f t} \langle J_I(0) P_I(t) \rangle dt \quad (\text{A11})$$

$$= \frac{i}{3Vk_B T \epsilon_0 2\pi f} \int_0^\infty \langle J_I(0) P_I(t) \rangle \frac{d}{dt} (e^{-2\pi i f t}) dt \quad (\text{A12})$$

$$\begin{aligned}&= \frac{i}{3Vk_B T \epsilon_0 2\pi f} \left[-\langle P_I(0) J_I(0) \rangle \right. \\ &\quad \left. - \int_0^\infty e^{-2\pi i f t} \langle J_I(0) J_I(t) \rangle dt \right]\end{aligned}$$

$$= -\frac{i}{3Vk_B T \epsilon_0 2\pi f} \int_0^\infty e^{-2\pi i f t} \langle J_I(0) J_I(t) \rangle dt \quad (\text{A13})$$

$$= -\frac{i}{2\pi f} \int_0^\infty e^{-2\pi i f t} \phi_I(t) dt, \quad (\text{A14})$$

where we used that $P_I(0)J_I(t)$ is odd under a time-reversal and thus $P_I(0)J_I(0) = 0$ in Eq. (A13). The imaginary part of $\chi_I(f)$ diverges in the low-frequency limit because of a finite ionic DC conductivity. The ionic conductivity $\sigma(f)$ is by convention the electric current response of free charges to an electric

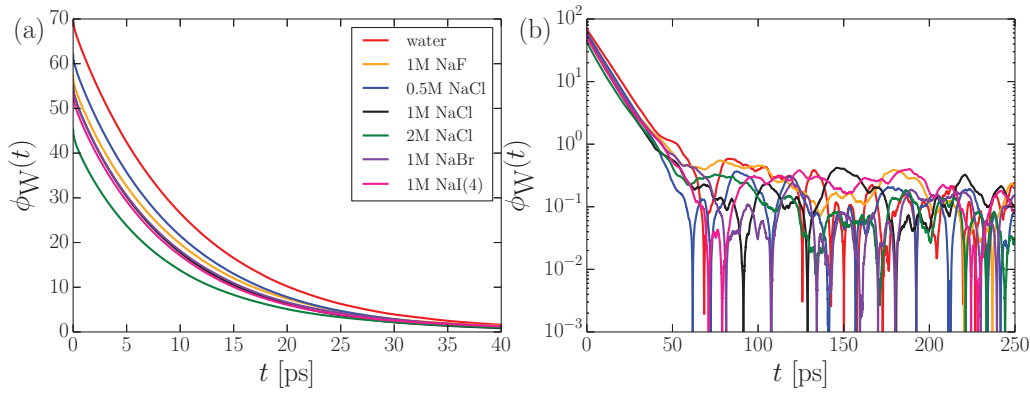


FIG. 8. (a) and (b) Auto-correlation function $\phi_W(t)$ of the water polarization. For all studied salt solutions, the data are strictly positive up to about 50 ps.

field,

$$\begin{aligned} \sigma(f) &= \frac{1}{3Vk_B T \epsilon_0} \int_0^\infty e^{-2\pi i f t} \langle J_1(t) \dot{P}(0) \rangle dt \\ &= \frac{1}{3Vk_B T \epsilon_0} \int_0^\infty e^{-2\pi i f t} \langle J_1(0) \dot{P}(t) \rangle dt \end{aligned} \quad (\text{A15})$$

$$\begin{aligned} &= \frac{1}{3Vk_B T \epsilon_0} \int_0^\infty e^{-2\pi i f t} \langle J_1(0) (\dot{P}_W(t) + \dot{P}_I(t)) \rangle dt \\ & \quad (\text{A16}) \end{aligned}$$

$$\begin{aligned} &= \frac{1}{3Vk_B T \epsilon_0} \left[\langle J_1(0) P_W(0) \rangle \right. \\ & \quad \left. - i2\pi f \int_0^\infty e^{-2\pi i f t} \langle P_W(0) J_1(t) \rangle dt \right. \\ & \quad \left. + \int_0^\infty e^{-2\pi i f t} \langle J_1(0) J_1(t) \rangle dt \right] \\ &= \frac{1}{3Vk_B T \epsilon_0} \left[-i2\pi f \int_0^\infty e^{-2\pi i f t} \langle P_W(0) J_1(t) \rangle dt \right. \\ & \quad \left. + \int_0^\infty e^{-2\pi i f t} \langle J_1(0) J_1(t) \rangle dt \right] \end{aligned} \quad (\text{A17})$$

$$= -i2\pi f \int_0^\infty e^{-2\pi i f t} \phi_{1W}(t) dt + \int_0^\infty e^{-2\pi i f t} \phi_1(t) dt. \quad (\text{A18})$$

By comparison with Eqs. (A9) and (A14) it is seen that $\sigma(f) = i2\pi f [\chi_1(f) + 0.5\chi_{1W}(f)]$. The static conductivity $\sigma_0 = \sigma(f = 0)$ depends only on the ion-current autocorrelation,

$$\sigma_0 = \frac{1}{3Vk_B T \epsilon_0} \int_0^\infty \langle J_1(0) J_1(t) \rangle dt = \int_0^\infty \phi_1(t) dt. \quad (\text{A19})$$

By adding the term $i\sigma_0/(2\pi f)$ to $\chi_1(f)$ the divergence is lifted and we obtain

$$\Delta\chi_1(f) = \chi_1(f) + i\sigma_0/(2\pi f) \quad (\text{A20})$$

$$= -\frac{i}{3Vk_B T \epsilon_0 2\pi f} \int_0^\infty (e^{-2\pi i f t} - 1) \langle J_1(0) J_1(t) \rangle dt. \quad (\text{A21})$$

The dielectric spectrum that is typically reported in experiments is the non-diverging expression $\Delta\chi(f) = \chi(f) + i\sigma_0/(2\pi f) = \chi_W(f) + \chi_{1W}(f) + \Delta\chi_1(f)$.

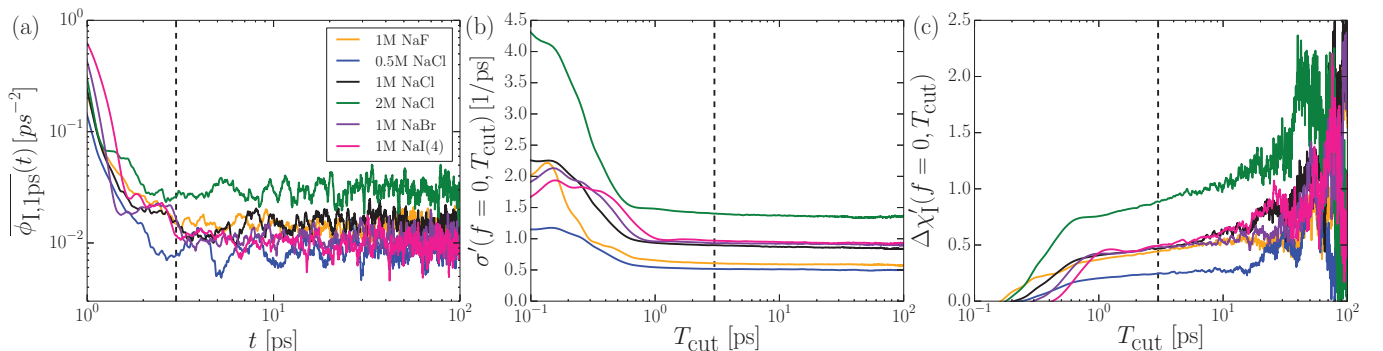


FIG. 9. (a) The running average over a time window of $T = 1$ ps of the absolute value of the ion polarization autocorrelation function $\phi_1(t)$ levels off at around $t = 3$ ps. (b) The static conductivity $\sigma'(f = 0, T_{\text{cut}})$ shows only weak dependence on the integration cutoff time T_{cut} . (c) The ion-polarization contribution to the static dielectric constant, $\Delta\chi_1'(f = 0, T_{\text{cut}})$ exhibits considerable dependence on the integration cutoff time T_{cut} .

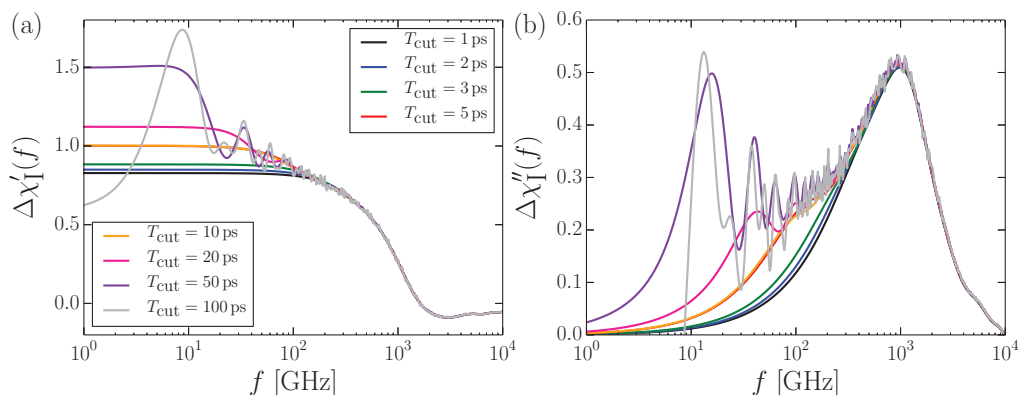


FIG. 10. (a) and (b) The ion-polarization contribution to the dielectric spectrum $\Delta\chi'_I(f)$ for 2 M NaCl is shown for various integration cutoff times T_{cut} . For larger cutoff times, the spectrum exhibits additional features in the low-frequency range.

APPENDIX B: INTEGRATION OF THE CORRELATION FUNCTIONS

The water polarization auto-correlation function $\phi_W(t)$, the ion current auto-correlation function $\phi_I(t)$, and the cross-correlation function between the ion current and water polarization $\phi_{IW}(t)$ are obtained using fast Fourier-transformation techniques. Since all correlation functions decrease with time they drop below the noise level at finite time, it is therefore useful to use an integration cutoff during calculation of the spectra via Laplace transformation. In the following, the choice of the cutoff-time T_{cut} for the different correlation functions is discussed.

1. Water polarization auto-correlation

The water polarization auto-correlation function $\phi_W(t)$ is most relevant for the computation of the dielectric spectra. Because of noise, $\phi_W(t)$ drops below zero between 50 and 200 ps for all studied solutions, as demonstrated in Figure 8. Therefore, we integrate $\phi_W(t)$ only up to the time threshold where it first drops below zero.

2. Ion-water cross-correlation function

The ion-water cross-correlation function $\phi_{IW}(t)$ is zero at $t = 0$, reaches a maximum after about 0.2 ps and then drops to

zero within about 20 ps. Similar to $\phi_W(t)$ we integrate $\phi_{IW}(t)$ up to the time threshold where it first drops below zero.

3. Ion current auto-correlation

Since the ion current auto-correlation function $\phi_I(t)$ oscillates, we cannot use the first drop below zero to determine a cutoff time. We denote the running average of $\phi_I(t)$ over a time window T by

$$\overline{\phi_{I,T}}(t) = \int_{t-0.5T}^{t+0.5T} |\phi_I(t')| \frac{dt'}{T}. \quad (\text{B1})$$

Figure 9(a) shows that the $T = 1$ ps average of $\phi_I(t)$ only decreases until about 3 ps beyond which it levels off because of noise. Therefore, we choose a cutoff of $T_{\text{cut}} = 3$ ps to limit the influence of noise on the dielectric spectra. To check the influence of the chosen cutoff we calculate the ionic contribution to the static conductivity $\sigma'_I(f = 0, T_{\text{cut}})$ and to the static dielectric constant $\Delta\chi'_I(f = 0, T_{\text{cut}})$ as a function of the integration cutoff T_{cut} , the results are shown in Figures 9(b) and 9(c). The cutoff is not critical for the conductivity $\sigma'_I(f = 0)$, because only the short-time behavior of $\phi_I(t)$ is relevant, the results for $\Delta\chi'_I(f = 0)$ more sensitively depend on the cutoff parameter and become noisy for larger cutoff values. To investigate the cutoff effects on $\Delta\chi'_I$ further, we in Figure 10 show

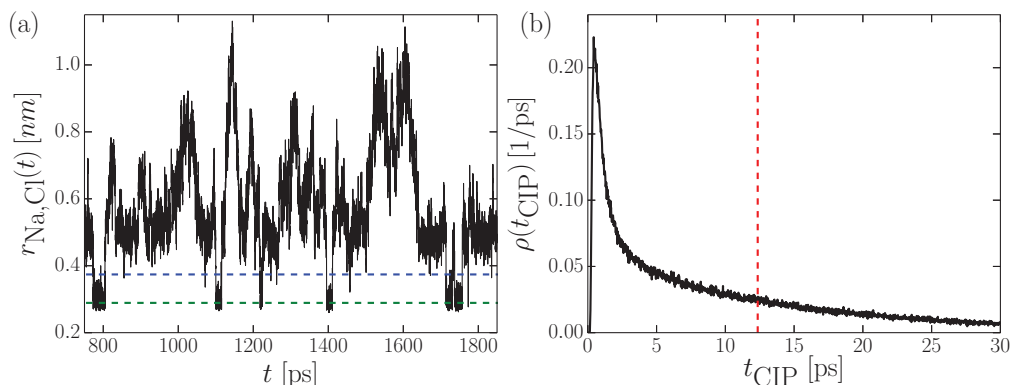


FIG. 11. (a) Trajectory of the distance $r_{\text{Na,Cl}}(t)$ between a sodium ion in 1 M NaCl solution and the closest chloride ion (black line). The dashed blue line is the threshold between CIP and SIP and the dashed green line shows the position of the maximum of the radial distribution function $g(r_{\text{Na,Cl}})$ (shown in Fig. 1(c)). (b) Probability distribution of the CIP lifetime t_{CIP} .

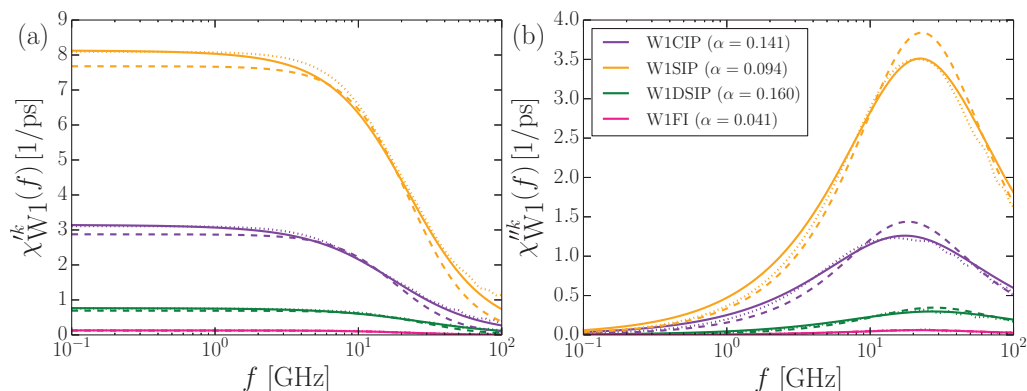


FIG. 12. Decomposition of the first solvation shell water contribution to the dielectric spectrum, $\chi_{W1}(f)$, for 2 M NaCl into separate contributions from solvation water of contact ion pairs (CIP, purple), solvent-separated ion pairs (SIP, orange), doubly solvent separated ion pairs (DSIP, green), and free ions (FI, pink). Simulation data are shown by dots, single Debye fits by dashed lines, and Cole-Cole fits by solid lines.

the spectral function for various cutoffs. For the larger cutoff values, low-frequency features appear which cannot easily be distinguished from noise. Therefore, we have to acknowledge that low-frequency ionic processes cannot be ruled out based on our simulation data, since the auto-correlation function $\phi_1(t)$ is only statistically robust for the first ps. This is no problem for the total dielectric spectra, since the ion polarization autocorrelation only contributes negligibly, but for the complete understanding of low-frequency ionic polarization effects much longer simulations would be necessary.

APPENDIX C: CONTACT ION PAIR LIFETIME

In Figure 11(a), we present a typical time evolution of the distance $r_{\text{Na,Cl}}(t)$ between a sodium ion in 1 M NaCl solution and the closest chloride ion (black line). According to our definition in Sec. II B, contact ion pairs are pairs with distance r smaller than the threshold $r_{\text{CIP}} = 0.374$ nm (dashed blue line). If t_0 and $t_1 > t_0$ are times with $r(t_0) = r(t_1) = r_{\text{CIP}}$ and $r(t) \leq r_{\text{CIP}}$ for all $t \in [t_0, t_1]$, the CIP lifetime is defined as the difference $t_1 - t_0$. In order to exclude jumps around the threshold, we only include strongly bound pairs where at least once in the range $[t_0, t_1]$ the distance is below $r_0 = 0.289$ nm (dashed green line), where r_0 is the position of the maximum of the radial distribution function $g(r_{\text{Na,Cl}})$ (shown in Fig. 1(c)). So the CIP lifetime can be expressed as

$$t_{\text{CIP}} = (t_1 - t_0) | t_1 > t_0, r(t_0) = r(t_1) = r_{\text{CIP}}, \\ r(t) \leq r_{\text{CIP}} \forall t \in [t_0, t_1], \min(r(t)) | t \in [t_0, t_1] < r_0.$$

The probability distribution of t_{CIP} is shown in Figure 12(b) and has an average value of 12.3 ps (red line).

Since the mean lifetime of ion pairs is of the order of the relaxation time of water, it is clear that sodium-halide ion pairs are difficult to probe based on dielectric spectroscopy.

APPENDIX D: COLE-COLE VS. SINGLE DEBYE FITS

Figures 4(a) and 4(b) in the main text demonstrate that the spectral contribution of the first solvation shell $\chi_{W1}(f)$ of a 2 M NaCl solution is not Debye-like and characterized by a rather large Cole-Cole exponent of $\alpha = 0.112$. A further

decomposition of the spectral contribution from the first solvation shell depending on the pair configuration of the closest ion according to

$$\chi_{W1}(f) = \chi_{W1\text{CIP}}(f) + \chi_{W1\text{SIP}}(f) + \chi_{W1\text{DSIP}}(f) + \chi_{W1\text{FI}}(f)$$

is shown in Figure 12. Here, the simulation data are shown by dots, single-Debye fits by broken lines, and Cole-Cole fits by solid lines. It is seen that the Debye fits perform rather poorly, in fact, some of the exponents for the individual contributions are even larger than the Cole-Cole exponent for the entire first-solvation shell ensemble. This means that the large deviations of the dielectric contribution due to first solvation shell water from single-Debye behavior is not a signature of different ionic environments which each are characterized by different relaxation times.

- ¹R. Buchner and G. Hefter, *PCCP* **11**, 8984 (2009).
- ²R. Buchner, G. T. Hefter, and J. Barthel, *J. Chem. Soc., Faraday Trans.* **90**, 2475 (1994).
- ³R. Buchner, G. T. Hefter, and P. M. May, *J. Phys. Chem. A* **103**, 1 (1999).
- ⁴W. Wachter, W. Kunz, R. Buchner, and G. Hefter, *J. Phys. Chem. A* **109**, 8675 (2005).
- ⁵A. Chandra, *J. Chem. Phys.* **113**, 903 (2000).
- ⁶S. Chowdhuri and A. Chandra, *J. Chem. Phys.* **115**, 3732 (2001).
- ⁷A. Y. Zasetky and I. M. Svishchev, *J. Chem. Phys.* **115**, 1448 (2001).
- ⁸A. Knocks and H. Weingärtner, *J. Phys. Chem. B* **105**, 3635 (2001).
- ⁹C. Schröder, T. Rudas, and O. Steinhauser, *J. Chem. Phys.* **125**, 244506 (2006).
- ¹⁰C. Schröder, C. Wakai, H. Weingärtner, and O. Steinhauser, *J. Chem. Phys.* **126**, 084511 (2007).
- ¹¹J. Sala, E. Guardia, and J. Marti, *J. Chem. Phys.* **132**, 214505 (2010).
- ¹²C. Schröder and O. Steinhauser, *J. Chem. Phys.* **132**, 244109 (2010).
- ¹³M. Sega, S. Kantorovich, C. Holm, and A. Arnold, *J. Chem. Phys.* **140**, 211101 (2014).
- ¹⁴H. Weingärtner, A. Knocks, S. Boresch, P. Höchtl, and O. Steinhauser, *J. Chem. Phys.* **115**, 1463 (2001).
- ¹⁵J. Holzmann, R. Ludwig, A. Geiger, and D. Paschek, *Angew. Chem., Int. Ed.* **46**, 8907 (2007).
- ¹⁶K. J. Tielrooij, N. Garcia-Araez, M. Bonn, and H. J. Bakker, *Science* **328**, 1006 (2010).
- ¹⁷J. T. O'Brien, J. S. Prell, M. F. Bush, and E. R. Williams, *J. Am. Chem. Soc.* **132**, 8248 (2010).
- ¹⁸S. Funkner, G. Niehues, D. A. Schmidt, M. Heyden, G. Schwaab, K. M. Callahan, D. J. Tobias, and M. Havenith, *J. Am. Chem. Soc.* **134**, 1030 (2011).
- ¹⁹F. Kohler, G. Findenegg, J. Fischer, and H. Posch, *The Liquid State* (Verlag Chemie Weinheim, 1972).

- ²⁰S. De Groot and P. Mazur, *Non-equilibrium Thermodynamics* (Dover, New York, 1984), pp. 150–156.
- ²¹J. M. Caillol, D. Levesque, and J. J. Weis, *J. Chem. Phys.* **85**, 6645 (1986).
- ²²I. Kalcher and J. Dzubiella, *J. Chem. Phys.* **130**, 134507 (2009).
- ²³C. J. Fennell, A. Bizjak, V. Vlachy, and K. A. Dill, *J. Phys. Chem. B* **113**, 6782 (2009).
- ²⁴B. Hess, C. Kutzner, D. van der Spoel, and E. Lindahl, *J. Chem. Theory Comput.* **4**, 435 (2008).
- ²⁵H. Berendsen, J. Grigera, and T. Straatsma, *J. Phys. Chem.* **91**, 6269 (1987).
- ²⁶M. Fyta and R. R. Netz, *J. Chem. Phys.* **136**, 124103 (2012).
- ²⁷U. Kaatz, *Z. Phys. Chem.* **135**, 51 (1983).
- ²⁸Y. Marcus, *Chem. Rev.* **88**, 1475 (1988).
- ²⁹H. E. Alper and R. M. Levy, *J. Phys. Chem.* **94**, 8401 (1990).
- ³⁰P. J. Lenart, A. Jusufi, and A. Z. Panagiotopoulos, *J. Chem. Phys.* **126**, 044509 (2007).
- ³¹M. Rami Reddy and M. Berkowitz, *Chem. Phys. Lett.* **155**, 173 (1989).
- ³²J. Martí, E. Guàrdia, and J. Padró, *J. Chem. Phys.* **101**, 10883 (1994).
- ³³F. Sedlmeier and R. R. Netz, *J. Chem. Phys.* **138**, 115101 (2013).
- ³⁴P. Madden and D. Kivelson, *Adv. Chem. Phys.* **56**, 467 (1984).
- ³⁵J. G. Kirkwood, *J. Chem. Phys.* **7**, 911 (1939).
- ³⁶P. E. Smith and W. F. van Gunsteren, *J. Chem. Phys.* **100**, 3169 (1994).
- ³⁷M. Sega, S. Kantorovich, and A. Arnold, “Kinetic dielectric decrement revisited: phenomenology of finite ion concentrations,” *Phys. Chem. Chem. Phys.* (published online 2014).
- ³⁸J. F. Chambers, J. M. Stokes, and R. H. Stokes, *J. Phys. Chem.* **60**, 985 (1956).
- ³⁹L. Onsager, *Phys. Z.* **27**, 388 (1926).